<div align="center">

Retroreflector Array Transfer Functions
by
David A. Arnold

</div>

<div align="center">

94 Pierce Road
Watertown, MA 02472-3035
617-924-6812

</div>

Contents

1. Introduction

The theme of this conference is "Toward Millimeter Accuracy". There are a number of effects that can cause systematic errors in laser ranging at the millimeter level. These effects are difficult to see in orbital analysis but can be calculated analytically using computer models of the retroreflector array and the laser ranging system.

The data shown in this report has been calculated theoretically. Some of the results are confirmed by experimental data. The rest would required additional experiments to verify whether the analysis is correct.

Some of this work was funded by NASA. The rest was done privately as part of an informal proposal for funding to participate in the activities of the Signal Processing working group. The results of this proposal effort are being presented at this conference to illustrate the kinds of problems that can be studied and the results that can be obtained relative to the goal of achieving millimeter accuracy. The computer models that have been developed are described in Appendix A.

2. Diffraction patterns of single cube corners.

A. Diffraction patterns of a coated circular cube corner.
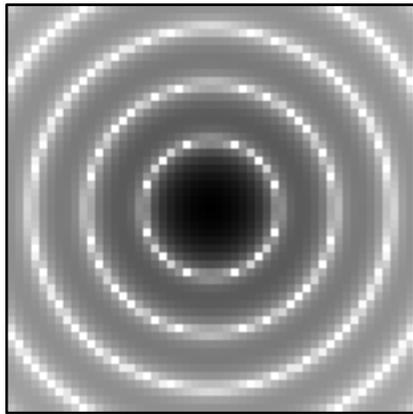
(A) No Dihedral
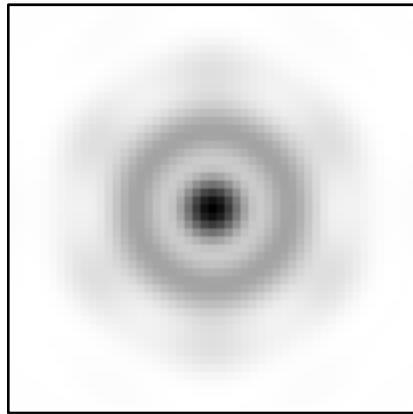
(B) On first ring
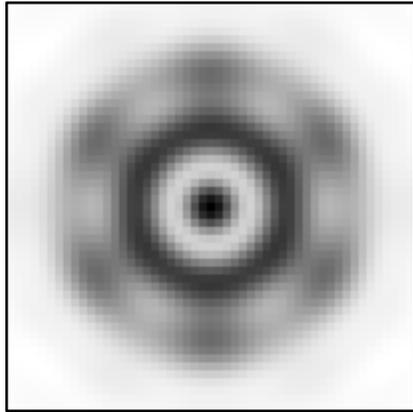
(C) Between rings 1 & 2
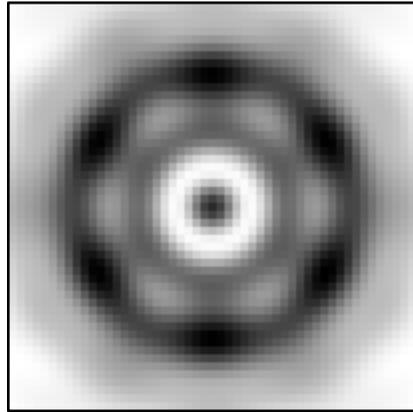
(D) On second ring
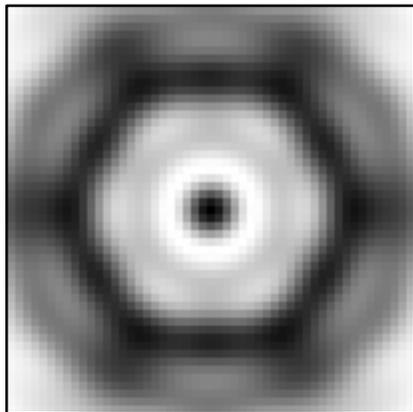
(E) Between rings 2 & 3
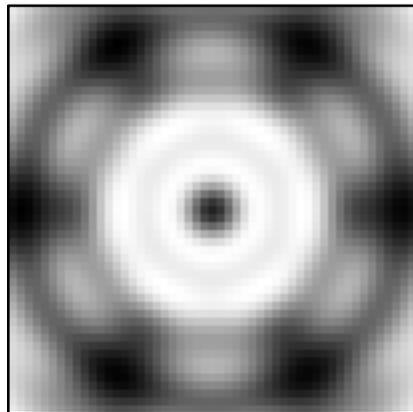
(F) On third ring

Figure 1. Coated 1.5 inch cube corner with various dihedral angle offsets.

Figure 1 shows some diffraction patterns of a perfect circular coated 1.5 inch cube corner with index of refraction n =1.461 for different dihedral angle offsets. The size of the plots is from -50 to +50 microradians in both dimensions. The patterns are displayed as inverted gray scale plots. Part (A) is a logarithmic plot. Parts (B) - (F) are linear plots.

The beam spread γ if the three dihedral angles of a cube corner are offset by an angle δ is given by the equation

$$\gamma = \frac{4}{3}\sqrt{6}n\delta \tag{1}$$

where n is the index of refraction. At normal incidence the geometrical optics solution is six spots in the form of a hexagon.

Part (A) of the figure shows the diffraction pattern with no dihedral angle offset. The diffraction pattern is displayed as a logarithmic plot in order to show the rings. In a linear plot, only the central lobe would be visible. The three rings are at 22.82, 37.40 and 51.63 microradians.

Part (B) shows the diffraction pattern with a dihedral angle offset .986 arc seconds. Using equation (1) for this offset gives a beam spread of 22.82 microradians, the same as the first ring. Because of diffraction effects, the six spots that would exits in the geometrical optics solution coalesce into a smooth ring.

In part (C) the dihedral angle of 1.30 arc seconds is trying to create spots between the first and second rings. The pattern shows hexagonal symmetry outside the first ring.

In part (D) the dihedral angle of 1.62 arc seconds gives a beam spread from equation (1) of 37.40 microradians, the same as the radius of the second diffraction ring. The second ring is the brightest, but is not as smooth as the first ring.

In part (E) the dihedral angle of 1.92 arc sec is trying to put spots between the second and third rings. The pattern is more complicated.

In part (F) the dihedral angle offset of 2.2 arc seconds gives a beam spread from equation (1) of 51.63 arc sec, the same as the third diffraction ring. The third ring is the brightest and there are six spots at the position of the geometrical optics solution.

B. Diffraction patterns of an uncoated circular cube corner.

Figure 2 shows diffraction patterns of a 1.5 inch diameter circular uncoated cube corner. The first column (left) shows the total energy. The second column (middle) shows the component of the reflected energy that is in the same (parallel) polarization state as the input. The third column (right) shows the energy in the orthogonal component. The first column is the sum of columns two and three.

Parts (A), (B), and (C) of figure 2 are for circular polarization with no dihedral angle offset. Part (B) has triangular symmetry and the energy is primarily in the central lobe. Part (C) has hexagonal symmetry and the energy is primarily in the ring of six spots. The total energy in part (A) does not have perfect hexagonal symmetry, but there are six spots around the central lobe that are approximately in the shape of a hexagon.

Circular polarization

No dihedral angle offset
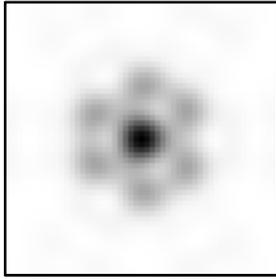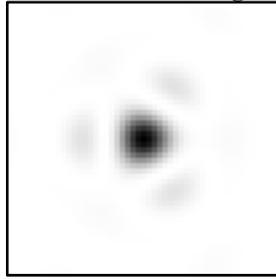
(A) Total energy (B) Parallel component (C) Orthogonal Component
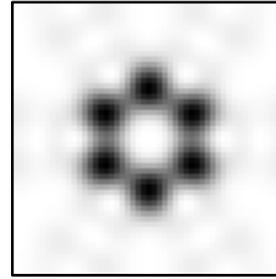
Dihedral angle offset 1.25 arc seconds
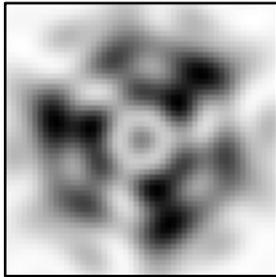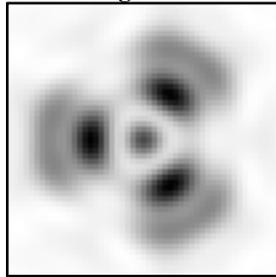
(D) Total energy (E) Parallel component (F) Orthogonal Component
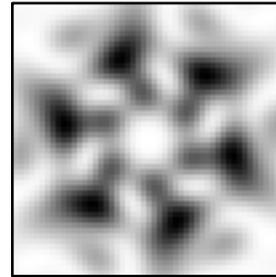
Linear vertical polarization

No dihedral angle offset
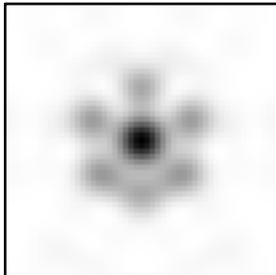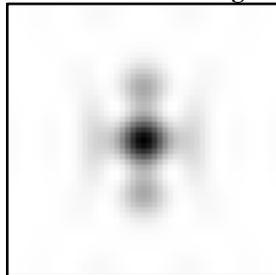
(G) Total energy (H) Parallel component (I) Orthogonal Component
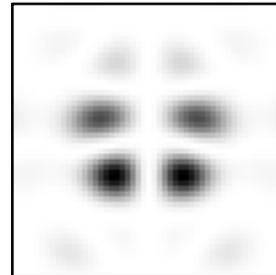
Dihedral angle offset 1.25 arc seconds
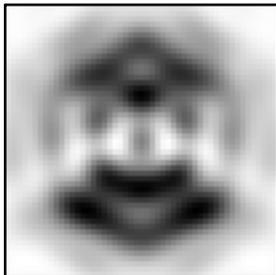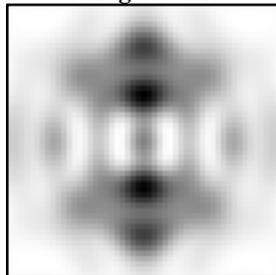
(J) Total energy (K) Parallel component (L) Orthogonal Component
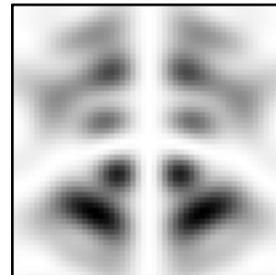
Figure 2. Diffraction pattern of an uncoated 1.5 inch cube corner with, and without, a dihedral angle offset, for circular and linear input polarization.

Parts (D), (E), and (F) are for circular polarization with a dihedral angle offset.

Parts (G), (H), and (I) are with linear vertical polarization and no dihedral angle offset. Parts (H), and (I) show symmetry from left to right. The total energy in part (G) has six spots around the central lobe that are approximately in the shape of a hexagon with left to right symmetry. Parts (G), (H), and (I) have been observed experimentally (see figures 3, 4, and 5 of reference 1).

Parts (J), (K), and (L) are for linear polarization with a dihedral angle offset. There is an interaction between the linear polarization and the dihedral angle offset that creates a "dumbbell" type pattern aligned with the polarization vector. The patterns show left to right symmetry.

With no dihedral angle offset the total energy as shown in parts (A) and (G) has a nearly hexagonal shape. With a dihedral angle offset, the total energy for circular polarization has approximately circular symmetry. The total energy for linear polarization has a "dumbbell" shape.

In an array of cube corners with no dihedral angle offset, the six spots around the central peak can be made into a reasonably smooth ring by having a distribution of orientations for the cube corners. However, this cannot be done with a dihedral angle offset and linear polarization because the interaction between the polarization and the dihedral angle offset produces a "dumbbell" shaped pattern aligned with the polarization vector.

3. Basic principles of retroreflector array design.

A. Geometry of the array.

For a single cube corner, the range correction can be calculated to a high degree of accuracy from the index of refraction and the angle of incidence. However, a single cube may not provide adequate signal strength or adequate angular coverage.

For a planar array of identical cubes all at the same orientation, the range correction will be the same as that of a single cube at the center of mass of the array. In practice, manufacturing imperfections cause variations in the reflecting properties of different cubes that can cause changes in the range correction.

The diffraction pattern of a cube corner depends on the incidence angle. For an array of cubes at different orientations (such as a spherical array), the range correction will be different at each point in the far field diffraction pattern.

B. Size of the array

A single retroreflector acts like a point reflector. There is no pulse spreading and no uncertainty in the range correction. If the target consists of a number of cube corners at different distances along the line of sight, there will be spreading of the pulse. In order to minimize range uncertainties, the range depth of the array should be kept as small as possible.

C. Velocity aberration and diffraction.

Because of velocity aberration, the center of the return beam is deflected away from the source by the angle $2v/c$ where v is the component of the satellite's velocity perpendicular to the line of sight. The signal at the receiver will depend on the intensity of the diffraction pattern of the cube corners at an angle $2v/c$ from the center of the return beam. Having a smooth diffraction pattern at $2v/c$ will minimize the variations in the cross section and range correction.

The smoothest part of the diffraction pattern is the central lobe. For a coated cube corner the first zero is at 1.22 λ/D where λ is the wavelength and D is the diameter of the cube corner. In low earth orbit, the cube corner would have to be quite small to put the receiver on the central lobe. Using the first ring as in Figure 1(B) would also produce a smooth pattern with a coated cube corner and allow the use of a larger cube.

Uncoated cubes have a natural beam spread with six spots around the central lobe. This is the result of polarization effects caused by total internal reflection at the back faces. The beam is wider than for a coated cube without the need for a dihedral angle offset.

D. Thermal gradients

The diffraction pattern of a cube corner can be severely degraded by thermal gradients in the material. The larger the cube corner the greater the sensitivity to thermal gradients because of the longer optical path lengths and the larger total temperature difference for a particular gradient. With a linear vertical temperature gradient the effect on the central irradiance of a coated cube corner is proportional to the square of the diameter of the cube corner. Another problem in coated cube corners is absorption of sunlight at the metalized back reflecting faces.

E. Dihedral angle offsets.

It is difficult (and expensive) to manufacture a cube corner with a specific dihedral angle offset. The smaller the tolerance the greater the cost. A tolerance less than .5 arc seconds could result in a lot of cube corners being rejected or re-manufactured.

One reason for having a specific dihedral angle offset is to be able to model the transfer function of the array. For the purposes of modeling it does not really matter what the dihedral angle is as long as its value is known. Measuring and recording the angles can be more cost effective than setting tight tolerances as long at the angles are within the range needed to achieve the necessary beam spread.

F. Coated vs uncoated cube corners.

The choice of coated or uncoated cubes will depend on the requirements. Some of the properties to be considered are the following:

a. Uncoated cube corners lose total internal reflection starting at about 17 degrees incidence angle. In a spherical satellite this has the effect of reducing the range depth. Having less range depth reduces the pulse spreading, coherent variations, and possible variations in range correction.

b. The reflection from an uncoated cube corner has energy in both polarization components regardless of the input polarization. Coherent interference occurs only within each polarization component. In other words, the x component cannot interfere with the y component and vice versa. This results in better averaging of coherent interference by a factor of $\sqrt{2}$.

c. Uncoated cubes have a higher reflectivity at normal incidence than coated cubes because of total internal reflection. The helps to compensate for the loss of signal past the cutoff angle for total internal reflection so as to produce a stronger signal with less range depth.

d. Uncoated cubes have no back faces to absorb solar radiation and contribute to thermal gradients.

e. Uncoated cubes have no back faces that could peel or be subject to deterioration over long periods of time.

f. The natural beam spread in an uncoated cube can eliminate the need for a dihedral angle offset. There is a cost advantage to specifying the dihedral angle as 90 degrees with some tolerance. A negative dihedral angle offset produces about the same pattern as a positive dihedral angle offset. Specifying the dihedral angle as 90 degrees with a tolerance of 1/2 arc second gives the same consistency of performance as specifying the angle as 90 degrees plus 1/4 arc second with a tolerance of 1/4 arc second.

g. The cutoff angle in an uncoated cube corner can vary from about 17 degrees to the normal cutoff of about 57 degrees depending on the orientation of the cube corner. To avoid anomalies in the transfer function for a spherical satellite it is necessary to have a distribution of orientations of the cube corners. A distribution of orientations is also desirable to smooth out the pattern since there are six spots outside the central lobe.

h. If linear polarization is used the transfer function with uncoated cubes has a "dumbbell" shape which can introduce a systematic error if no correction is applied. The problem can be corrected by applying a correction for the asymmetry. The asymmetry can be eliminated by using circular polarization.

4. Transfer function of the Lageos retroreflector array.

The design goal for Lageos was 5 millimeters. To that level of accuracy the range correction can be considered constant. The peak to peak variations in the centroid range correction can be as large as + or - 5 millimeters. The transfer function of the Lageos retroreflector array is given in reference 2. The method of calculation is described in reference 3.

A. Cross section and range correction at a single orientation

The computer capabilities available in 1978 when reference 2 was published were very limited compared to what is available today. I have recalculated and re-plotted some of the figures from reference 2. The results are shown in figure 3.

Linear **Circular**

(A) (B)
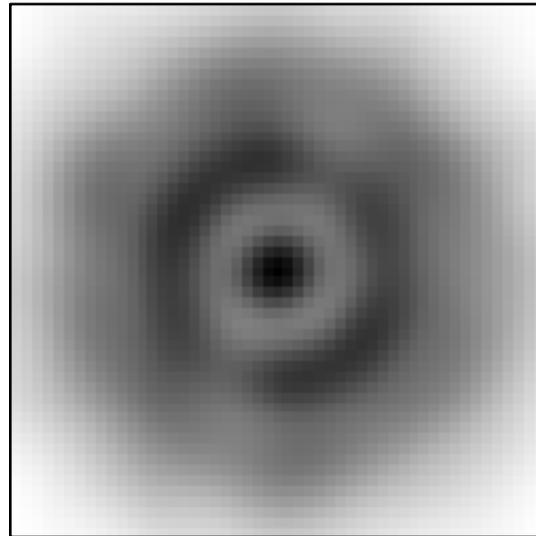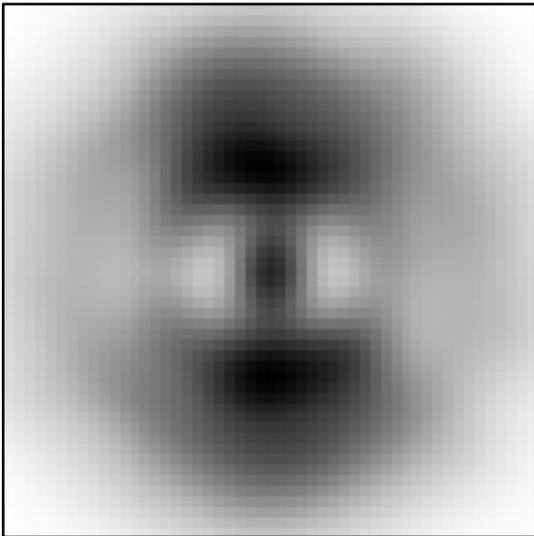
Centroid range correction
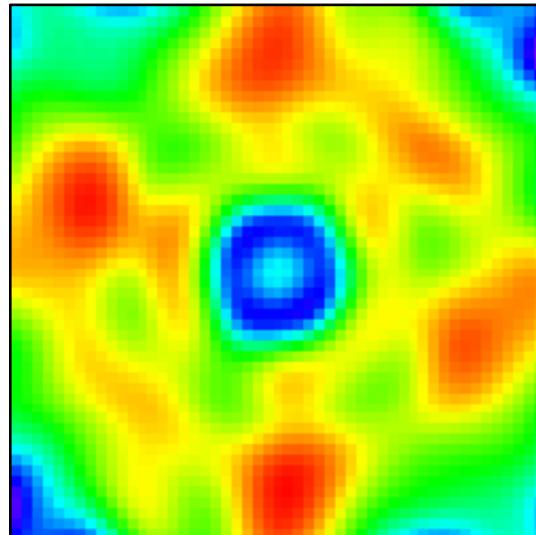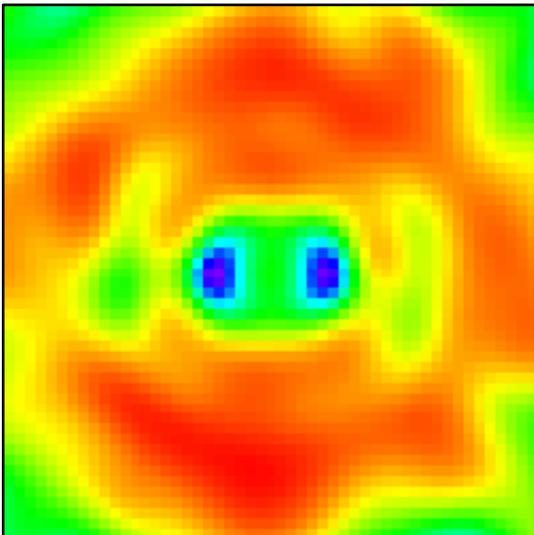
Linear **Circular**

(C) (D)

Figure 3. Cross section and range correction for linear vertical polarization and circular polarization. The satellite orientation angle is $\theta = 20$ deg, and $\phi = 150$ degrees. The dihedral angle offset is 1.25 arc seconds. The wavelength is 532 nanometers.

The correspondence between the figures in reference 2 and figure 3 of this report is as follows:

Reference 2	This report
Figure 9-2	Figure 3(A)
Figure 9-10	Figure 3(B)
Figure 10-2	Figure 3(C)
Figure 10-10	Figure 3(D)

In reference 2 the diffraction pattern was calculated as a 21 x 21 matrix from -50 to +50 microradians in the far field. The 21 x 21 matrix which gives points only every 5 microradians was used to conserve computer time. The data was presented as a computer page plot with hand drawn contour lines.

In figure 3 of this report the pattern is calculated as a 51 x 51 matrix which gives points every 2 microradians. The cross section is presented as a gray scale plot and the centroid range correction matrix is presented as a rainbow plot with red for larger values and blue for smaller values. The incidence angle is $\theta = 20$ deg, and $\phi = 150$ deg.

Figure 3(A) shows that the cross section with linear polarization has a "dumbbell" shape. The cross section with circular polarization in part (B) has approximately circular symmetry. The centroid range correction matrices for linear polarization in part (C) and circular polarization in part (D) are more irregular and do not show a clear "dumbbell" or circular pattern.

The Lageos 2 retroreflector array was tested in the laboratory before launch and the results published in reference 4. At a meeting last year, one of the authors, Michael Selden, told me that the testing showed a difference in the range correction for Lageos between linear and circular polarization. He wanted to know if my theoretical analysis agreed with the experimental results.

As you can see from figure 3, the range correction matrix is different for linear and circular polarization. However, both are somewhat irregular at least as the particular orientation of the satellite used in the calculation.

B. Average cross section and range correction

In thinking about Michael Selden's question it seemed to me that the range correction should have circular symmetry for circular polarization and that the irregular shape in figure 3 might be due to the fact that there a limited number of retroreflectors active at a particular orientation of the satellite.

In order to test this idea I decided to do calculations at a number of orientations and average the results to see if the average range correction has well defined symmetry properties. The test used 16 orientations starting at $\theta = \phi = 0$ degrees and incrementing each angle by 5 degrees up to $\theta = \phi = 75$ degrees. The results are shown in figure 4.

Figure 4 shows that the average cross section and centroid range correction have a "dumbbell" shape for linear polarization and circular symmetry for circular polarization. The range correction for circular polarization still shows some irregularities in shape but is approaching circular symmetry.

## Cross section

**Linear**

Circular

(A)

(B)
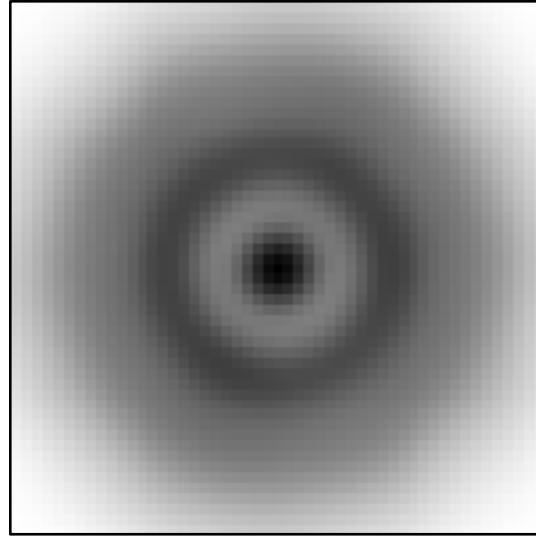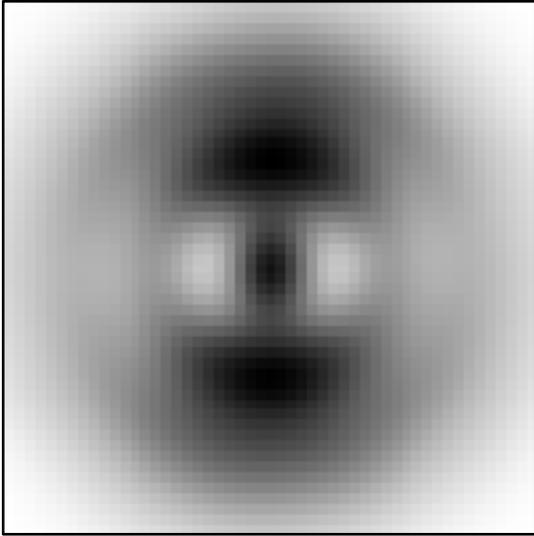
Centroid range correction
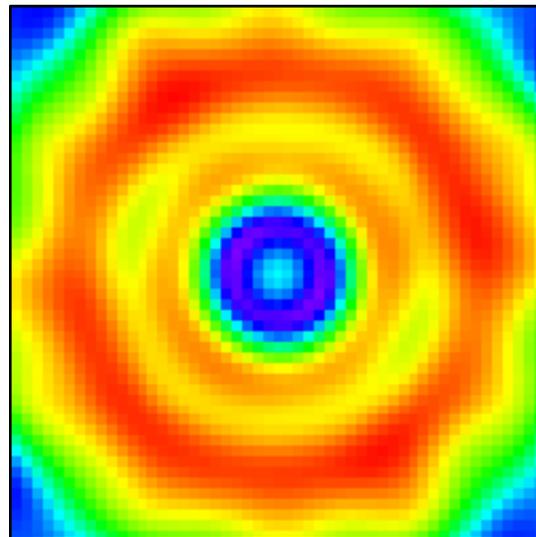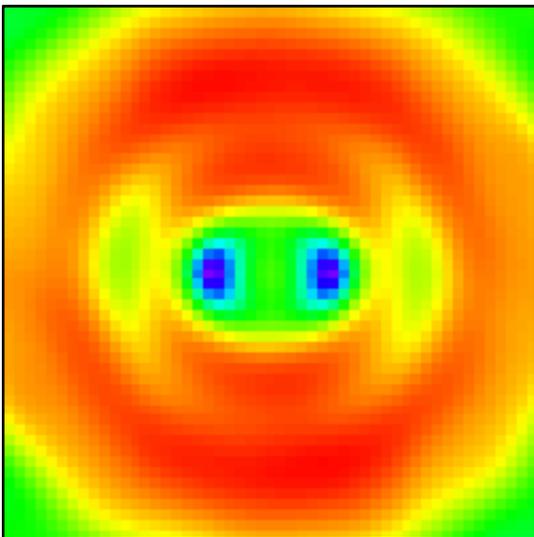
Linear

Circular

(C)

(D)

Figure 4. Cross section and range correction for linear vertical polarization and circular polarization. The cross section and range correction are averaged over 16 orientations. The dihedral angle offset is 1.25 arc seconds. The wavelength is 532 nanometers.
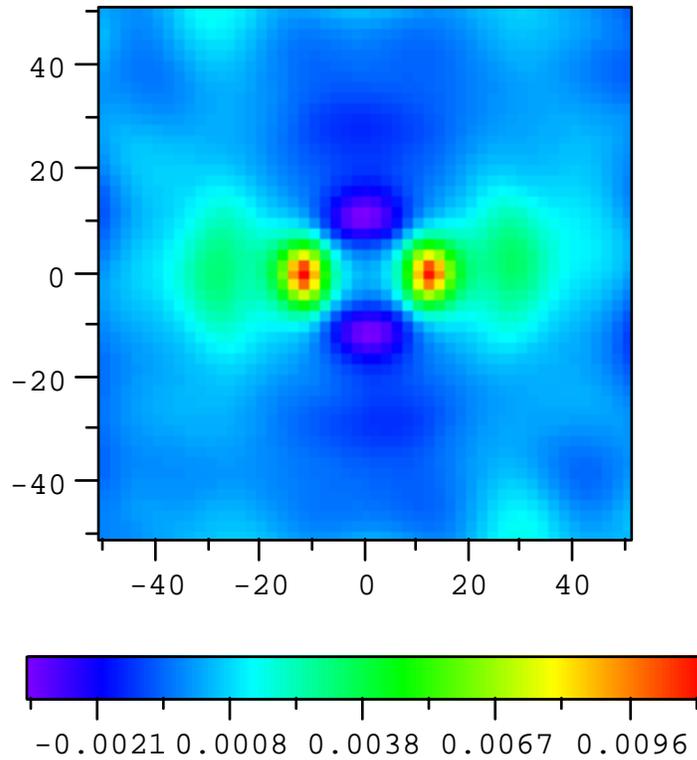
Microrad	Minimum	Average	Maximum	Max - Min
0.0	0.0002900	0.0002900	0.0002900	0.0000000
2.0	0.0001300	0.0002844	0.0004400	0.0003100
4.0	-0.0003500	0.0003055	0.0010100	0.0013600
6.0	-0.0012600	0.0004070	0.0023200	0.0035800
8.0	-0.0025000	0.0007455	0.0049800	0.0074800
10.0	-0.0035400	0.0013697	0.0088700	0.0124100
12.0	-0.0036900	0.0017901	0.0112100	0.0149000
14.0	-0.0030300	0.0015349	0.0093900	0.0124200
16.0	-0.0022200	0.0010137	0.0062200	0.0084400
18.0	-0.0016600	0.0006380	0.0040457	0.0057057
20.0	-0.0013800	0.0004527	0.0030525	0.0044325
22.0	-0.0013300	0.0003919	0.0027589	0.0040889
24.0	-0.0013900	0.0004026	0.0028730	0.0042630
26.0	-0.0014900	0.0004448	0.0031460	0.0046360
28.0	-0.0015300	0.0004764	0.0033378	0.0048678
30.0	-0.0014600	0.0004607	0.0032251	0.0046851
32.0	-0.0012962	0.0003913	0.0028010	0.0040972
34.0	-0.0011050	0.0003009	0.0022466	0.0033516
36.0	-0.0009526	0.0002213	0.0017655	0.0027181
38.0	-0.0008383	0.0001650	0.0014557	0.0022940
40.0	-0.0007818	0.0001302	0.0012738	0.0020556
42.0	-0.0007613	0.0001063	0.0011648	0.0019262
44.0	-0.0007415	0.0000879	0.0010549	0.0017964
46.0	-0.0007180	0.0000698	0.0008940	0.0016120
48.0	-0.0006269	0.0000507	0.0006611	0.0012880
50.0	-0.0008095	0.0000319	0.0007943	0.0016039

Figure 5. Centroid with circular polarization minus centroid with linear polarization averaged over 16 orientations.

Figure 5 shows the difference in the centroid range correction between linear and circular polarization. Since the pattern for circular polarization is circular and the pattern for linear polarization has left to right symmetry, the difference between the two patterns has left to right symmetry. It also has vertical symmetry (top to bottom).

The table under the color plot in figure 5 shows the value of the difference in range correction averaged around circles of increasing radius in the far field. Column 1 is the radius of the circle in microradians, column 2 is the minimum value around the circle, column 3 is the average, column 4 is the maximum value around the circle, and column 5 is the difference between the maximum and minimum values. In the interval from 32 to 38 microradians, the difference in the centroid range correction can vary by up to 4 millimeters. The effect is systematic and does not average out.

The asymmetry of the range correction for linear polarization will cause a systematic error in laser range data. For example, suppose the transmitted pulse has linear vertical polarization. The velocity aberration at culmination is approximately horizontal. This puts the receiver on the horizontal axis of the range correction matrix. The result is a distortion of the shape of a pass that does not go away no matter how many passes are averaged. The velocity aberration is nearly perpendicular to the line of sight at culmination. As a result the velocity aberration has its maximum value. This can cause a systematic error in the range correction for either linear or circular polarization.

C. Spinning satellite.

Both Lageos 1 and Lageos 2 were launched spinning. The spin rate decreases with time and is currently quite low for Lageos 1. Even if the satellite were not spinning, the viewing angle would vary throughout a pass as a result of the observing geometry.

Figure 6 shows the range correction for linear polarization at two points in the far field with the satellite spinning about its symmetry axis. The first point is on the vertical velocity aberration axis at $x = 0$, $y = 35$ microradians. The red curve is the centroid and the green curve is the half-max range correction. The second point is on the horizontal velocity aberration axis at $x = 35$, $y = 0$ microradians. The purple curve is the centroid and the blue curve is the half-max range correction. The range correction is always greater on the vertical axis. The average value of each range correction in millimeters is shown below.

Case	Average	rms	color
Centroid (0,35)	243.3	1.5	red
Centroid (35,0)	240.2	1.7	purple
Halfmax (0,35)	250.6	0.6	green
Halfmax (35,0)	249.9	0.7	blue
Centroid (both)	241.7	2.2	
Halfmax (both)	250.2	0.7	

The difference between the average centroid at the two points in the far field is 3.1 millimeters. The difference between the average half-max range corrections at the two points is .7 millimeters.

Figure 7 plots the difference between the range corrections at the two points in the far field. The red curve is for the centroid and the green curve is for half-max.

Range correction vs satellite rotation angle
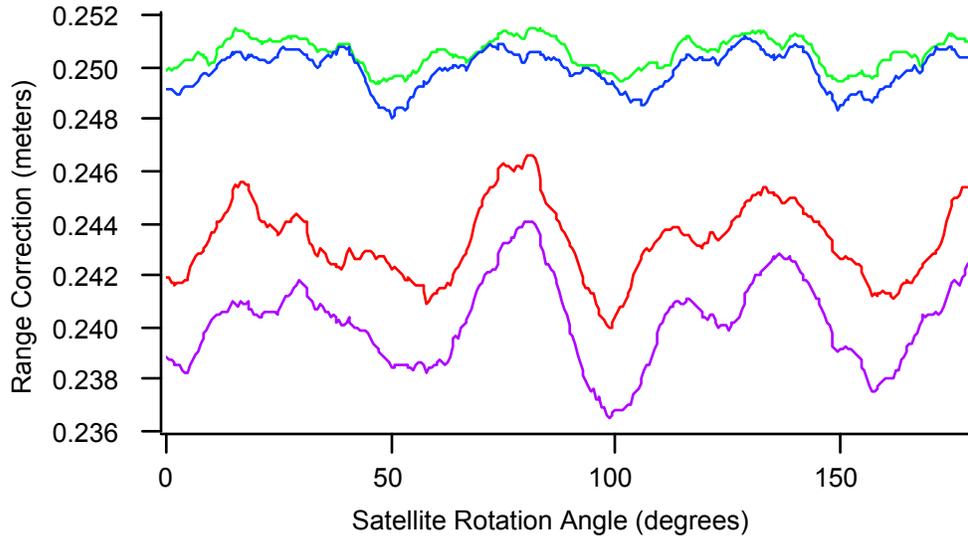
Figure 6. Centroid and half-max range correction vs satellite rotation angle at velocity aberration (0,35) and (35,0) µrad with linear vertical polarization (y-axis).
A. Velocity aberration x = 0 µrad, y = 35 µrad.
       red   = Centroid
       green = Half-max
B. Velocity aberration x = 35 µrad, y = 0 µrad
       Purple = Centroid
       Blue   = Half-max
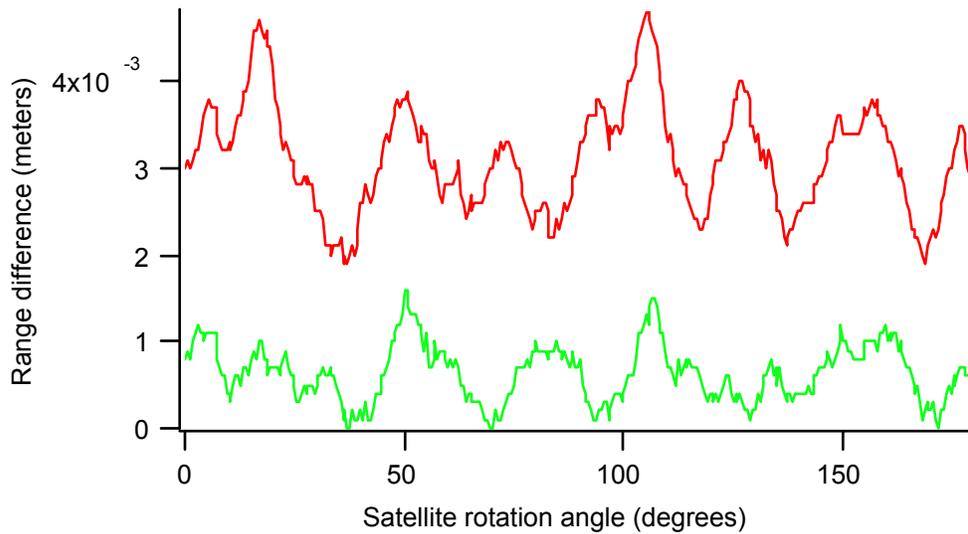
Figure 7. Range correction at (0,35) minus range correction at (35,0) µrad.
       Red   = centroid(0,35) - centroid(35,0)
       Green   = half-max(0,35) - half-max(35,0)

The variations in the half-max range correction are smaller than for the centroid since the half-max correction tends to measure the leading edge of the pulse. These calculations are for the incoherent case. They do not include the effects of coherence or photon quantization. These effects cause fluctuations in the range correction from pulse to pulse and can introduce a bias in multi-photoelectron measurements depending on the type of detection algorithm used.

D. Coherent variations of the range correction

Table 16 of the Lageos report in reference 2 presents some calculations of the coherent variation of various type of range correction for different pulse lengths.

Δ	σ	σ_m	Δ / σ_m
Centroid, Equal Weighting			
-2.16	8.67	0.43	-4.98
Centroid, Weighted by Signal Strength			
0.04	7.08	0.35	0.11
Half-Area, Equal Weighting			
-2.55	10.07	0.50	-5.06
Half-Area Weighted by Signal Strength			
-.82	7.72	0.39	-2.12
Half-Maximum, Equal Weighting			
-3.47	9.84	0.49	-7.06
Half-Maximum, Weighted by Signal Strength			
-2.54	6.93	0.35	-7.33

Table 1. Difference between the average range correction for a set of coherent returns and the range correction for the incoherent return. The pulse length is 200 nsec; Δ, σ, and σ_m are in millimeters. There are 400 returns in each sample; $\sigma_m = \sigma/20$.

Table 1 above shows the entries from table 16 in reference 2 for a pulse length of 200 picoseconds. In all but one of the cases, there is a statistically significant difference between the incoherent range correction and the average of the coherent range corrections.

The one exception is centroid detection with each measurement weighted by the signal strength. Since single photoelectron returns all have the same signal strength and measure the centroid, there should be no bias due to coherent variations. All the other types of measurements show a bias greater then 2 millimeters in this simulation for equal weighting. For half-max detection there is not much improvement when the returns are weighted by signal strength.

The calculations shown in table 1 do not model two effects which should decrease all of the variations. The first is that the calculation did not take into account the fact that there are two independent polarization states for each Lageos return because the cube corners are uncoated. Since each return is really two independent returns, the rms variations are probably smaller by a factor of $\sqrt{2}$ than what is listed in the table.

The second effect is that a pulse of finite length cannot be exactly monochromatic. This should further reduce the coherent variations. The coherent variation for centroid and half-max weighted by signal strength is about 7 millimeters. Dividing this by $\sqrt{2}$ gives 5 millimeters or less as an estimate of the coherent variations with a 200 picosecond pulse.

E. Signal strength dependence.

The signal processed by a laser receiving systems consists of a discrete number of photoelectrons. If the number of photoelectrons is large, the signal should be a good representation of the received signal. If the signal consists of a small number of photoelectrons, there will be variations in the shape of the pulse due to photon quantization.

For half-max detection systems, there will be a shift in the range correction as a function of signal strength. For single photoelectron returns, the average position of the photoelectron will be at the centroid of the retroreflector array. For half-max systems with a strong signal, the average measured position will be the half-max point on the leading edge of the pulse.

Figure 8 shows the results of a Lageos simulation with different pulse detection algorithms for average signal strengths from .1 to 1000 photoelectrons. The simulation is done for an orientation of the satellite where the centroid is 241 millimeters from the center of the array.

The rise time of the photo-multiplier is assumed to be .125 nanosecond and the half-max, half-width of a single photoelectron is 8.6 millimeters. For a photoelectron at the centroid the half-max point of the return is at 241 + 8.6 = 249.6 millimeters.

The transmitted pulse used in the simulation is 200 picoseconds which gives a one-way half-max, half width of 15 millimeters for the transmitted pulse. The half width of the return from the Lageos array (with a zero length input pulse) is about 21 millimeters. Convolving the transmitted pulse with the Lageos array and the photo-multiplier response gives a half width of about 27 millimeters for the return pulse. Adding this to the centroid of 241 millimeters gives a value of 268 millimeters for the half-max point on the return pulse for the strong signal case.

The top curve in blue in figure 8 is the average position of the half-max point on the return pulse vs signal strength. It starts out at 250 millimeters for single photoelectron returns and rises to 268 millimeters for strong signals. The green curve is the half-area point and the red curve (partially obscured by the green curve) is the centroid.

Figure 9 shows the variation of the range correction with signal strength for a set of target measurements. For the target measurements there is no spreading due to the target. The only spreading is due to the width of the transmitted pulse and the spreading of the photo-multiplier. This give a combined spreading of about 17 millimeters. Adding this to the centroid of 241 millimeters gives a half-max point of 258 millimeters for the strong signal case.

**Range correction vs average number of photoelectrons**
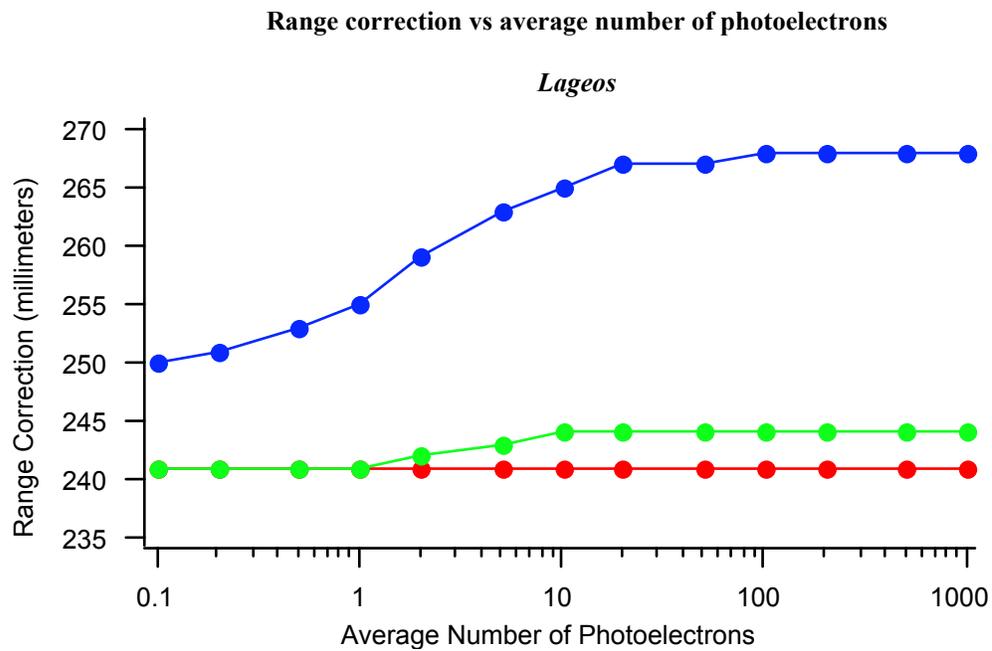
Lageos

Figure 8. Range correction for Lageos vs number of photoelectrons.
Blue = Half-Max
Green = Half Area
Red = Centroid
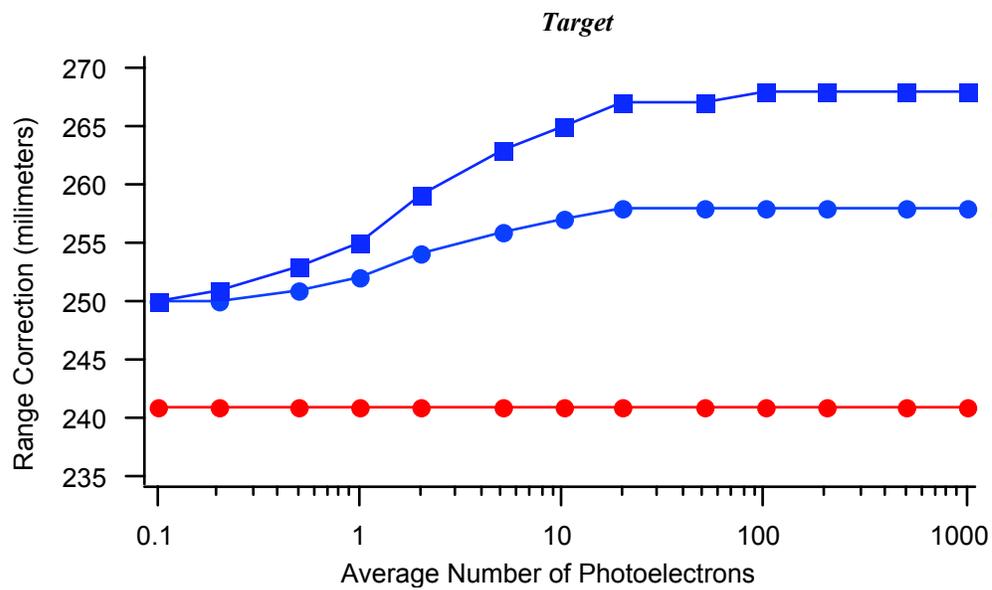
Target

Figure 9. Range correction for target calibration compared to Lageos Half-Max
Blue = Half-Max
Square = Lageos
Circle = Target
Red = Centroid and Half Area

The blue curve with circles in figure 9 is the position of the half-max point for the target measurements vs signal strength. The curve with blue squares is the half-max position for Lageos for comparison. The difference between the blue squares and the blue circles is the range correction that would need to be applied to Lageos range measurements as a function of signal strength. It is about 10 millimeters for this set of station parameters.

Appendix B shows the numerical data used to plot figures 8 and 9, describes the format of the tables, lists all the parameters used in the simulations, and gives a theoretical computation of the pulse spreading for comparison with the numerical simulation.

Appendix C gives a theoretical description of computer programs RETURN and LRSS which were used to do the signal strength simulations.

5. Transfer function of the TOPEX retroreflector array.

The retroreflector array on TOPEX/POSEIDON is larger than on many other satellites. The variations of the range correction with velocity aberration can be a few centimeters which is large enough to be seen in orbital analysis. In order to obtain adequate accuracy from satellite laser tracking it was necessary to compute the range correction as a function of velocity aberration at each incidence angle on the array.

Figure 10 shows cross section and range correction matrices for TOPEX from 0 to 60 degrees incidence angle. At 0 degrees the cross section has circular symmetry and the range correction is constant. At other incidence angles the pattern becomes asymmetrical. The asymmetry is the result of the dihedral angle offsets. The offset of each of the three back angles is 1.75 arc seconds. However, the divergence of the reflected spots depends on the order of reflection except at normal incidence.

Figure 11 shows the details of the cross section matrix at 40 degrees incidence angle. In the interval from 26 to 50 microradians the cross section can vary from a low of 171 to a high of 794 in the units used for plotting. The cross section is in units of $4\pi \times 10^4$ square meters.

Figure 12 shows the details of the centroid range correction at 40 degrees incidence angle. In the interval from 26 to 50 microradians the centroid can vary from a low of .466 to a high of .514 meters, a difference of almost 5 centimeters.

The centroid is relatively easy to compute and is unique. The intensity of the diffraction pattern of the ith cube corner at a point in the far field can be given as $S_i(\theta_1,\theta_2)$ where θ_1 and θ_2 are the components of the velocity aberration. The position along the line of sight is x_i. The centroid range correction is given by

$$R_i(\theta_1,\theta_2) = \frac{\sum_i S_i(\theta_1,\theta_2)x_i}{\sum_i S_i(\theta_1,\theta_2)}$$

For other types of detection systems such as half-max, the range correction must be computed by plotting the pulse shape at each point in the far field. The range correction will be different for each type of tracking system depending on the transmitted pulse length, receiver rise time, and method of detection.

TOPEX

Cross section

$\phi = 0$ $\phi = 10$ $\phi = 20$ $\phi = 30$

$\phi = 40$ $\phi = 50$ $\phi = 60$

Centroid

$\phi = 0$ $\phi = 10$ $\phi = 20$ $\phi = 30$

$\phi = 40$ $\phi = 50$ $\phi = 60$
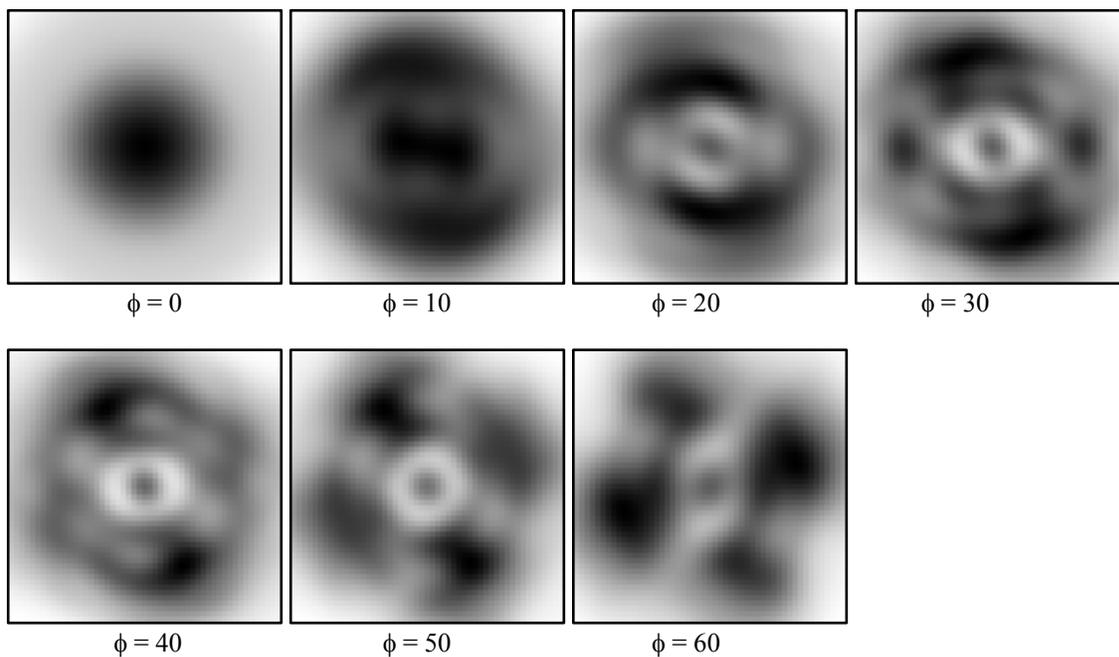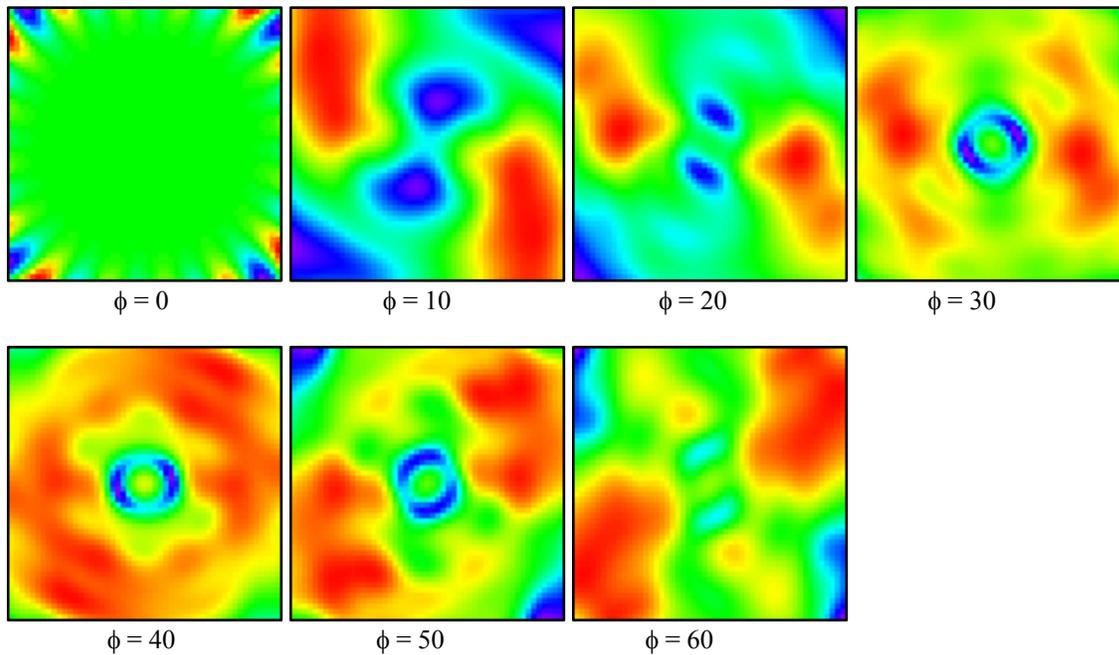
Figure 10. Topex cross section and centroid range correction vs incidence angle.
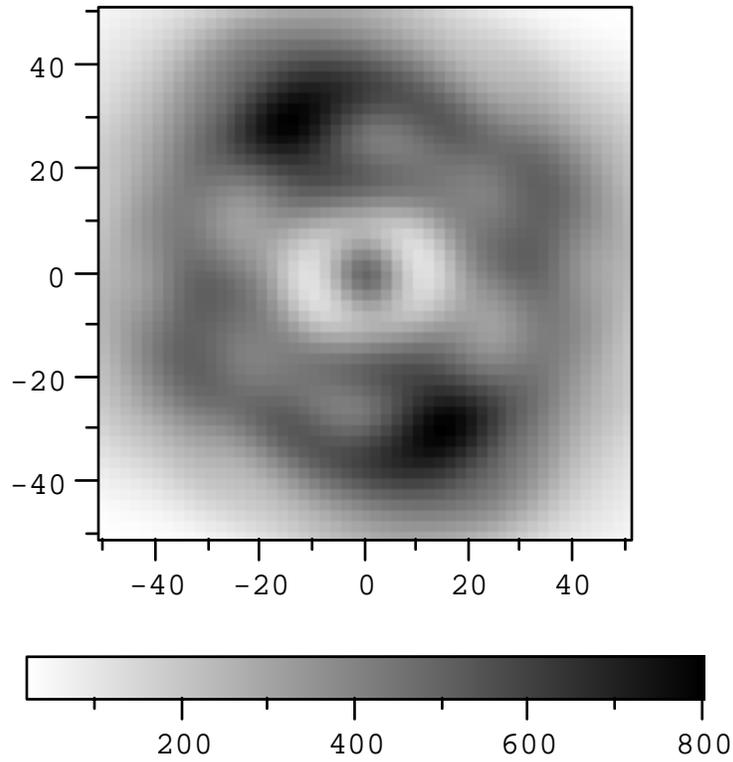
Microrad	Minimum	Average	Maximum	Max - Min
0.0	489.4849998	489.4849998	489.4849998	0.0000000
2.0	445.3091673	451.7482330	460.2240226	14.9148554
4.0	364.3271325	376.2008227	389.4566931	25.1295606
6.0	261.1307461	285.4701279	311.9223233	50.7915771
8.0	170.8840018	214.4467675	261.0669668	90.1829651
10.0	119.0825894	187.6761896	261.7588842	142.6762948
12.0	118.1161724	209.9228314	314.8369044	196.7207319
14.0	156.4614158	267.2486554	396.6649886	240.2035728
16.0	215.8758010	335.2755717	475.2044183	259.3286173
18.0	265.4050812	391.6353015	528.6968374	263.2917561
20.0	298.2786780	425.6962326	563.5087252	265.2300472
22.0	309.8627082	440.2211573	591.8992403	282.0365321
24.0	312.0507327	446.9562308	620.4357771	308.3850444
26.0	316.6035096	458.3720343	659.1760814	342.5725718
28.0	326.8786992	479.8423479	711.7925307	384.9138315
30.0	349.3779229	508.0959935	758.2196375	408.8417146
32.0	377.0046497	533.4914398	791.0682353	414.0635856
34.0	402.6764310	545.3260540	794.3722310	391.6958000
36.0	417.2127329	536.9520984	763.7709530	346.5582201
38.0	410.5974142	509.5386763	710.1096586	299.5122444
40.0	355.1654490	468.9192973	645.2657644	290.1003153
42.0	299.9186935	422.8592245	580.0306474	280.1119540
44.0	254.0910076	377.9353615	519.2259367	265.1349291
46.0	224.7911562	337.4302900	470.3656472	245.5744910
48.0	197.7001026	300.7906508	425.8873839	228.1872813
50.0	171.0913676	266.1335965	383.7737122	212.6823446

Figure 11. Topex cross section for $\phi = 40$ degrees incidence angle
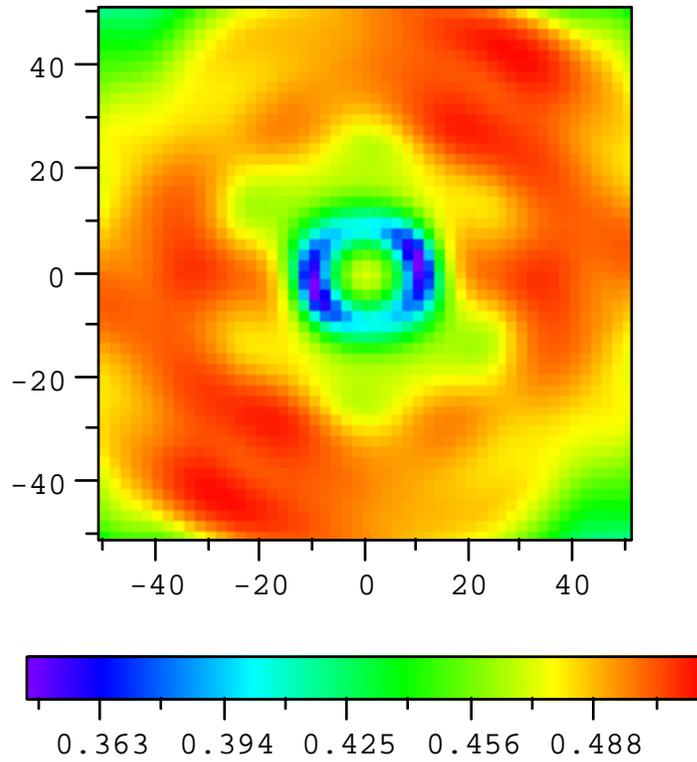
Microrad	Minimum	Average	Maximum	Max - Min
0.0	0.4724049	0.4724049	0.4724049	0.0000000
2.0	0.4666691	0.4673081	0.4687676	0.0020985
4.0	0.4523631	0.4539938	0.4566284	0.0042652
6.0	0.4257099	0.4293210	0.4320979	0.0063880
8.0	0.3839133	0.3970060	0.4074840	0.0235707
10.0	0.3470787	0.3792045	0.4040112	0.0569325
12.0	0.3677682	0.3979261	0.4228421	0.0550739
14.0	0.4164559	0.4323093	0.4444229	0.0279670
16.0	0.4441747	0.4568523	0.4678594	0.0236847
18.0	0.4573846	0.4696824	0.4867587	0.0293742
20.0	0.4629551	0.4753994	0.4949082	0.0319531
22.0	0.4642413	0.4777824	0.4982947	0.0340534
24.0	0.4640330	0.4796338	0.5003336	0.0363006
26.0	0.4658928	0.4828465	0.5022588	0.0363660
28.0	0.4696983	0.4875240	0.5045417	0.0348434
30.0	0.4761811	0.4926806	0.5068545	0.0306734
32.0	0.4824622	0.4969321	0.5110175	0.0285553
34.0	0.4868215	0.4995607	0.5122519	0.0254304
36.0	0.4884893	0.5004261	0.5110413	0.0225520
38.0	0.4872767	0.4999017	0.5084432	0.0211665
40.0	0.4848260	0.4985097	0.5070389	0.0222129
42.0	0.4823142	0.4968927	0.5052074	0.0228932
44.0	0.4808566	0.4956154	0.5047393	0.0238827
46.0	0.4804566	0.4948373	0.5079527	0.0274962
48.0	0.4791453	0.4941571	0.5119505	0.0328051
50.0	0.4766798	0.4930398	0.5144387	0.0377589

Figure 12. Topex centroid range correction (meters) at $\phi = 40$ degrees incidence angle.

For TOPEX, the diffraction pattern for each cube corner was computed at each incidence angle on the array along with the position along the line of sight. This was used to compute the range correction matrix at each incidence angle for each type of laser tracking system.

For TOPEX this procedure was necessary in order to achieve a tracking accuracy on the order of one centimeter. The variation of the range correction at different points in the far field is generally much smaller for other satellites and would probably not be obvious during orbital analysis.

In two-color ranging used to compute the atmospheric correction, it is necessary to have a much greater precision in the laser ranging than the accuracy desired for the atmospheric correction. For example, if the dispersion is a factor of 15, a one millimeter error in the range correction for the retroreflector array will cause an error of 1.5 centimeters in the atmospheric correction. The techniques developed for TOPEX could be used to increase the accuracy of the range correction for other satellites if the specifications of the retroreflectors are known,.

6. Transfer function of the WESTPAC retroreflector array

The WESTPAC satellite has hexagonal cube corners recessed in a cavity with a circular aperture. The method of calculating retroreflector array transfer functions described in reference 3 does not include the case of a recessed cube corner. However, the method has been extended to cover this particular case. It was possible to do this because the aperture of the cavity is smaller than the face of the cube corner so that the active reflecting area is determined only by the aperture. If the active reflecting area were the intersection of a circle and a hexagon, the analysis would have become extremely complicated.

Figure 13 shows the diffraction pattern of a recessed WESTPAC cube corner at incidence angle from 0 to 12 degrees at one degree intervals. The cutoff angle is 13 degrees so that the pattern at 13 degrees is zero. The diffraction patterns are shown as either a linear or logarithmic gray scale plot depending on which shows the details better. As the incidence angle increases, the pattern becomes more oval. Past 9 degrees the central lobe is wider than 50 microradians so that the receiver is always on the central lobe.

Since the satellite orientation is unknown, there is no way to calculate the cross section for a particular observation. The only available data that gives some information about the cross section is the magnitude of the velocity aberration. One thing that can be done with the diffraction patterns is to calculate the maximum possible cross section as a function of velocity aberration. The results of doing this are shown in figure 14.

In figure 14, the red curve is the maximum possible cross section as a function of velocity aberration with no dihedral angle offset. The WESTPAC cube corners are specified as having no dihedral angle offset within the manufacturing tolerances. The green curve shows the maximum possible cross section vs velocity aberration with a 1.75 arc second dihedral angle offset. The cross section is larger without a dihedral angle offset from 0 to 30 microradians velocity aberration. It is larger with a dihedral angle offset past 30 microradians.

Table 2 shows the data used to plot figure 14. Column 1 of the table is the velocity aberration, column 2 is the maximum cross section in the units used for plotting, column 3 is the incidence angle where the maximum occurs and column 4 is the maximum cross section in standard units. The data in column 2 is in units of $4\pi \times 10^4$ square meters.
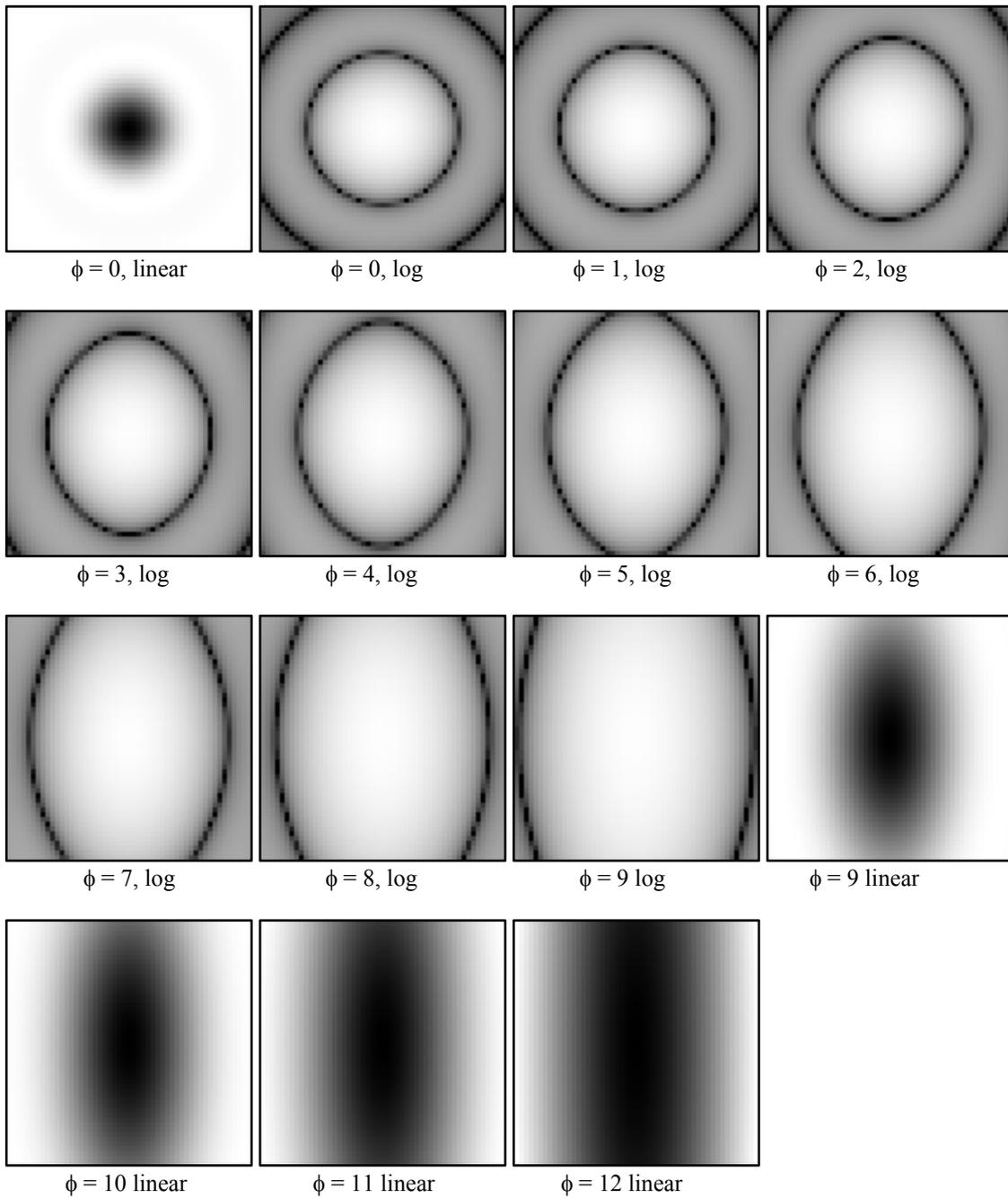
Figure 13. Cross section of a Westpac cube corner vs incidence angle in degrees. The cutoff angle is 13 degrees.

Maximum cross section for Westpac
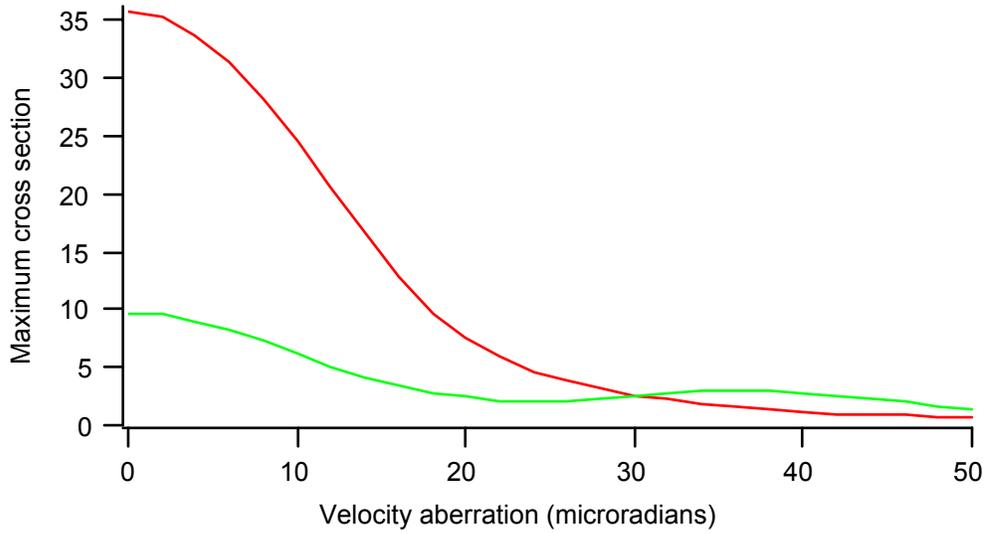
Figure 14. Maximum cross section vs velocity aberration for a Westpac cube corner.
Red   = No dihedral angle offset
Green = Dihedral angle 1.75 arc seconds

Microradians	Cross-section	angle (deg)	Cross Section (sq m)
0.0	35.8402293	0.0	2418805.6
2.0	35.3181832	0.0	2383573.5
4.0	33.7898797	0.0	2280430.5
6.0	31.3649939	0.0	2116778.4
8.0	28.2140207	0.0	1904123.7
10.0	24.5513900	0.0	1656938.1
12.0	20.6147328	0.0	1391258.7
14.0	16.6427276	0.0	1123193.8
16.0	12.8702210	0.0	868592.7
18.0	9.6913873	1.0	654057.8
20.0	7.4623938	2.0	503626.2
22.0	5.8602015	3.0	395496.6
24.0	4.6632240	4.0	314714.3
26.0	3.7767337	4.0	254886.3
28.0	3.1200028	5.0	210564.5
30.0	2.5685487	5.0	173347.7
32.0	2.1777955	6.0	146976.3
34.0	1.8420879	6.0	124319.9
36.0	1.5592573	7.0	105232.0
38.0	1.3636733	7.0	92032.4
40.0	1.1796034	7.0	79609.7
42.0	1.0083017	7.0	68048.8
44.0	0.8980635	8.0	60609.0
46.0	0.8019726	8.0	54124.0
48.0	0.7107092	8.0	47964.7
50.0	0.6246997	8.0	42160.1

Table 2. Maximum cross section vs velocity aberration with no dihedral angle offset. Column 1 is the velocity aberration, column 2 is the cross section in units of 4π x 10,000 sq meters, column 3 is the incidence angle where the maximum occurs, and column 4 is the cross section in sq meters.

With no dihedral angle offset the maximum cross section in the interval from 26 to 50 microradians in table 2 is about 255,000 square meters in standard units. The published value of the measured cross section for WESTPAC is in the range 200,000 to 300,000 square meters.

Table 3 shows a sample of the data from which the maximum cross section was determined and Table 4 is the maximum cross section with a 1.75 arc second dihedral angle offset.

Microrad	Minimum	Average	Maximum	Max - Min
26.0	0.7717976	1.5842181	2.6464027	1.8746051
28.0	0.5466180	1.3367811	2.4216995	1.8750815
30.0	0.3655866	1.1131764	2.1982273	1.8326407
32.0	0.2268892	0.9147052	1.9784917	1.7516025
34.0	0.1268098	0.7419771	1.7648064	1.6379966
36.0	0.0602277	0.5954080	1.5592573	1.4990296
38.0	0.0211537	0.4723924	1.3636733	1.3425196
40.0	0.0032599	0.3711284	1.1796034	1.1763435
42.0	0.0003617	0.2896156	1.0083017	1.0079400
44.0	0.0005316	0.2254193	0.8507194	0.8501879
46.0	0.0008714	0.1759270	0.7075042	0.7066328
48.0	0.0017305	0.1378011	0.5790063	0.5772758
50.0	0.0020692	0.1094539	0.4652917	0.4632225

Table 3. Cross section for Westpac at 7 deg incidence angle with no dihedral angle offset . The maximum values for velocity aberration 36, 38, 40, and 42 microradians are the values shown in column 2 of table 2.

Microradians	Cross-section	angle (deg)	Cross Section (sq m)
0.0	9.7185625	0.0	655891.8
2.0	9.5451555	0.0	644188.8
4.0	9.0422200	0.0	610246.4
6.0	8.2595189	0.0	557423.1
8.0	7.2731369	0.0	490853.6
10.0	6.1761959	0.0	416822.6
12.0	5.0703650	0.0	342191.7
14.0	4.1527559	1.0	280263.5
16.0	3.3936579	2.0	229033.1
18.0	2.8364401	2.0	191427.3
20.0	2.4167251	2.0	163101.3
22.0	2.1403943	2.0	144452.1
24.0	1.9977891	2.0	134827.9
26.0	2.0994745	0.0	141690.5
28.0	2.3420730	0.0	158063.1
30.0	2.6136478	0.0	176391.3
32.0	2.8498785	0.0	192334.2
34.0	3.0019057	0.0	202594.3
36.0	3.0466102	0.0	205611.3
38.0	2.9844830	0.0	201418.5
40.0	2.8160866	0.0	190053.6
42.0	2.5648466	0.0	173097.8
44.0	2.2631820	0.0	152738.9
46.0	1.9465926	0.0	131372.7
48.0	1.6624684	1.0	112197.6
50.0	1.4361345	1.0	96922.7

Table 4. Maximum cross section vs velocity aberration for WESTPAC with a dihedral angle offset of 1.75 arc seconds.

References

1. OPTICAL PROPERTIES OF THE APOLLO LASER RANGING RETROREFLECTOR ARRAYS, R.F Chang, C.O. Alley, D.G. Currie, and J.E. Faller, Space Research XII, Akademie-Verlag, Berlin, 1972.

2. OPTICAL AND INFRARED TRANSFER FUNCTION OF THE LAGEOS RETROREFLECTOR ARRAY, Grant NGR 09-015-002, David A. Arnold, May, 1978.

3. METHOD OF CALCULATING RETROREFLECTOR-ARRAY TRANSFER FUNCTIONS, David A. Arnold, Smithsonian Astrophysical Observatory SPECIAL REPORT 382.

4. Prelauch Optical Characterization of the Laser Geodynamic Satellite (LAGEOS 2), Peter O. Minott, Thomas W. Zagwodzki, Thomas Varghese, and Michael Selden.

Acknowledgments

Appendix A. Description of analysis programs

 The original versions of these programs were written in the early 70's. The current versions have a number of new features that have been added recently.

TRANSFR   This program is described in SAO Special Report 382. It is optimized for computing an N x N diffraction pattern of an array. Matrices for cross section, centroid range correction, and pulse spread (r.m.s width) are computed. The program has been recently updated to include recessed cube corners such as used on WESTPAC.

RETURN   This program is like TRANSFR except that it uses versions of the diffraction subroutines that compute only a single point in the far field. The pulse shape is computed to determine the centroid, half-area, peak, and half-max points. The program can also model coherent interference and photon quantization using a random number generator. The program has been recently recreated after not being used for 25 years. Some work remains to be done to get the program fully operational.

LRSS   (Laser Receiving System Simulation). This program can use a pulse shape computed by RETURN or generate a Gaussian input pulse. The average number of photoelectrons is used to generate random signal strengths using a Poisson distribution. Photoelectrons are randomly distributed in the area under the pulse. The pulse shape is plotted and analyzed for various detection algorithms - centroid, half-area, half-max, and pulse analyzer (with a centroid algorithm). The program was recently recreated after not being used for 25 years.

DIFRACT This program computes the diffraction program of a single cube corner at normal incidence by numerical integration of a 101 x 101 array of phases. It can model the effect of a temperature gradient expressed as a quadratic function in three dimensions with origin at the center of the front face. New features have been added to model various types of curvature of the wavefront expressed as a polynomial function of the position from the center of the front face. Modification have been added to produce phase plots, and simulated interferograms.

ECCENTRIC This program computes signal strength in photoelectrons for a specific set of station parameters for a satellite in an eccentric orbit. It is a recently written program based on an old program, RNGEQN, which modeled only circular orbits. The cross section of the satellite can be given as a constant, a table vs velocity aberration, or a two-dimensional matrix. The program can accept a set of matrices vs incidence angle on the array assuming the satellite is gravity gradient stabilized. The cross section matrices are computed by program TRANSFR

Appendix B. Tables for signal strength dependence of the Lageos range correction.

Lageos

Average PE	No. of pulses	Cent	RMS	Half area	RMS	1/2 max	RMS	Returns
.1	10000	241	21.9	241	21.9	250	22.1	964
.2	10000	241	21.3	241	21.3	251	21.6	1816
.5	10000	241	20.7	241	20.7	253	21.2	3949
1.0	10000	241	19.4	241	19.4	255	20.2	6312
2.0	5000	241	16.8	242	16.8	259	17.9	4337
5.0	2000	241	11.0	243	11.1	263	12.3	1991
10.0	1000	241	7.5	244	7.7	265	8.8	999
20.0	500	241	5.2	244	5.0	267	6.3	500
50.0	200	241	3.2	244	3.0	267	3.9	200
100.0	100	241	2.1	244	1.9	268	2.8	100
200.0	50	241	1.5	244	1.3	268	2.2	50
500.0	20	241	.9	244	.9	268	1.4	20
1000.0	10	241	.8	244	.7	268	1.0	10

Average PE	No. of pulses	Returns vs. Photoelectrons 1	2	3	4	5	6	7
.1	10000	906	56	2				
.2	10000	1623	179	14				
.5	10000	3021	763	144	20	1		
1.0	10000	3655	1825	626	163	34	8	1
2.0	5000	1377	1373	869	432	188	68	23
5.0	2000	69	162	276	355	357	301	199
10.0	1000	1	0	7	21	42	60	86
20.0	500	0	0	0	0	0	0	0
50.0	200	0	0	0	0	0	0	0
100.0	100	0	0	0	0	0	0	0
200.0	50	0	0	0	0	0	0	0
500.0	20	0	0	0	0	0	0	0
1000.0	10	0	0	0	0	0	0	0

Pulse shape from LAGEOS computed with program RETURN. Laser pulse width .2 ns. Centroid 241 mm. Half-area 244 mm. Half-max point on pulse at 266 mm. Half-max range correction $241 + 10 = 251$ mm. Output pulse sigma (r.m.s. width) 22 mm.

Format of the Lageos tables

First Table

Column Data

Average PE	The average signal strength in photoelectrons. A specific number of photoelectrons for each pulse is chosen using a Poisson distribution.
No. of pulses	Number of pulses to be generated and averaged.
Cent	Average centroid of all the pulses in millimeters
RMS	'sigma' or r.m.s variation of the centroid values (mm)
Half area	Average Half area range correction (mm)
RMS	r.m.s variation of the Half Area range corrections (mm)
1/2 max	Average half-max position on the leading edge of the pulses
RMS	r.m.s variation of the 1/2 max positions
Returns	Number of pulses having at least one photoelectron

Second Table

Column	Data
Average PE	Average number of photoelectrons
No. of pulses	Number of pulses to generate
Returns vs. Photoelectrons	Number of returns having 1,2,3,4,5,6,7 photoelectrons

Note: For average signal strengths past 1.0, there are pulses having more than 7 photoelectrons in the sample. These are not listed.

Target Calibration

Average PE	No. of pulses	Cent	RMS	Half area	RMS	1/2 max	RMS	Returns
.1	10000	241	12.7	241	12.7	250	12.9	964
.2	10000	241	12.6	241	12.4	250	12.7	1816
.5	10000	241	11.9	241	11.9	251	12.5	3949
1.0	10000	241	11.5	241	11.5	252	12.6	6312
2.0	5000	241	10.3	241	10.4	254	11.9	4337
5.0	2000	241	6.0	241	6.6	256	8.7	1991
10.0	1000	241	4.5	241	4.6	257	6.5	999
20.0	500	241	3.0	241	3.1	258	4.6	500
50.0	200	241	1.9	241	1.9	258	2.9	200
100.0	100	241	1.1	241	1.3	258	2.1	100
200.0	50	241	.8	241	.9	258	1.6	50
500.0	20	241	.6	241	.6	258	1.0	20
1000.0	10	241	.5	241	.5	258	.7	10

Pulse shape from target computed with program RETURN. Single cube with range correction 241 mm. Laser pulse width .2 ns. Half-area 241 mm. Half-max point on pulse at 256 mm. Half-max range correction 241 mm. Output pulse sigma (r.m.s width) 12.8 mm.

Input Parameters for program LRSS

Data   **Description**

Data	Description
5	Number of fixed threshholds (.1, .2, .5, 1.0, 2.0 Volts - data not shown in tables)
.2	Laser pulse width (FWHM) (Not used - use input pulse shape from RETURN)
.125	Photo-multiplier rise time (ns). Sigma = .125/(2 x 1.28) = .0488 ns.
.050	Single photoelectron voltage
.1	Attenuation factor
30.	Amplifier gain
0.	Amplifier rise time (ns)
9999.	Amplifier cutoff (dummy - not used)
1.	Counter gain
0.	Counter rise time (ns)
.005	Pulse shape plot interval (ns) for numerical analysis
8.	Pulse analyzer channel to center on half-max point of leading edge
.07	Channel separation (ns)
.025	Channel width (ns)
40	Number of channels
<.3	Amplifier linear region (volts)
.3-2.7	Amplifier distortion (volts)
>2.7	Amplifier saturation (volts)

Average amplifier input .25 volts for 100 photoelectrons. Pulses with more than 100 photoelectrons in distorted region of amplifier. No distortion model used.

Analyzer uses centroid algorithm. Range corrections (not shown) same as Centroid.

Analytical calculation of pulse width and rms noise

PHOTOMULTIPLIER

For a .125 ns rise time of the photomultiplier the sigma of a single photoelectron should be .125/(2 x 1.28) = .0488 ns. (I do not remember where the factor of 1.28 comes from.) In one-way meters this is .0488 x .3/2 = .0732 meters or 7.3 mm. The half-max point on a single photoelectron is 7.32 x 1.1774 = 8.6 mm from the center. The factor of 1.1774 is the square root of ln(4). The average position of a single photoelectron is the centroid. With the center of a photoelectron at 241 mm, the half-max point should be at 241 + 8.6 = 249.6 mm in agreement with the value of 250 mm in the simulations for single photoelectrons.

TARGET CALIBRATION

For a .2 ns laser pulse the one way half-max point should be 15 mm from the center. With the center at 241 mm the half-max point should be at 241 + 15 = 256 mm. Convolving the 15 mm from the laser pulse with the 8.6 mm from the photomultiplier gives a half-max point about 17 mm from the center. The convolution is SQRT(15**2 + 8.6**2) for two Gaussians. Adding 241 and 17 gives 258 in agreement with the target calibration simulation for strong signals.

LAGEOS RETURN PULSE

The half-max point on the LAGEOS return pulse as computed by program RETURN is at 266 mm. After going through the photomultiplier it is at about 268 mm. If the laser pulse has zero width, the sigma of the return from LAGEOS is about 18 mm (or a half-max point of 18 x 1.1774 = 21 mm). Convolving 21 mm for the array with 15 mm for the laser pulse gives a half-max point of SQRT(21**2 + 15**2) = 26 mm from the center. Adding 241 and 26 gives 267 in approximate agreement with the half-max point of 266 mm computed by program RETURN. Since the return pulse is asymmetrical the convolution should be done numerically. The square root of the sum of the squares gives only an approximate answer.

RANGE VARIATIONS DUE TO QUANTIZATION

For a .2 ns laser pulse the one way half-max point is 15 mm from the center. The standard deviation (sigma) of the pulse is 15/1.1774 = 12.7 mm. This agrees with the single photoelectron RMS scatter in the target calibration table. The pulse sigma calculated for LAGEOS by program RETURN for a .2 ns pulse is 22 mm. This agrees with the RMS scatter for a single photoelectron in the LAGEOS table. The sigma of the return from LAGEOS with a zero width pulse is 18 mm. Convolving this with the 12.7 mm sigma for a .2 ns pulse gives SQRT(18**2 + 12.7**2) = 22 mm in agreement with the value calculated by program RETURN. This formula can be used to calculate the single photoelectron scatter for other laser pulse widths.

Appendix C. Theory of programs RETURN and LRSS

1. The intensity of the transmitted laser pulse as a function of position along the beam is assumed to be

$$I(x) = \frac{1}{\sigma\sqrt{2\pi}} e^{-\frac{x^2}{2\sigma^2}}$$

where σ(meters) = pulse width (nsec) × .3/(2 × 1.1774).

2. The retroreflector array is defined by giving the position and orientation of each reflector with respect to the centroid of the satellite in the orbital configuration.

3. The energy reflected from each cube corner can be computed in either of two ways. In the first it is proportional to the active reflecting area of the retroreflector which is a function of the angle of incidence of the laser pulse on the front face of the retroreflector. In the second it is given by the cross section of the retroreflector at a particular point in the far field diffraction pattern. The second method is more precise.

4. The coherent return from the satellite array is computed by assigning random phases to the reflection from each cube corner. The reflected intensity is

$$I_R(x) = A(x)A^*(x)$$

where

$$A(x) = \sum_{i=1}^{N} \sqrt{\frac{S_i}{\sigma\sqrt{2\pi}}} e^{-\frac{(x-d_i)^2}{4\sigma^2}} e^{j\theta_i}$$

with S_i = active reflecting area or cross section of each cube corner

d_i = twice the distance of the reflector from the centroid of the satellite along the

line of sight

θ_i = the random phase angle assigned to each cube corner

σ = the sigma of the transmitted pulse

N = the number of retroreflectors

$j = \sqrt{-1}$

5. The average number $\bar{n}_I$ of photoelectrons per pulse is chosen arbitrarily in the system simulation program. Let E_c be the energy of a coherent pulse and E_I be the energy of the incoherent return. The average value of E_c is E_I. The average number $\bar{n}_c$ of photoelectrons generated by a coherent pulse of energy E_c is

$$\bar{n}_c = \bar{n}_I \frac{E_c}{E_I}$$

The actual number n of photoelectrons received will fluctuate about the value $\bar{n}_c$ according to a Poisson distribution. Using a random number generator giving numbers uniformly distributed on the interval 0 to 1 one can pick a value for n as follows. The normalized probability of a value k of the variable n is

$$P_{\bar{n}_c}(k) = \frac{\bar{n}_c^k}{k!} e^{-\bar{n}_c}$$

For a random number R, the corresponding value of n is the smallest value of n for which

$$\sum_{k=0}^{n} P_{\bar{n}_c}(k) > R$$

6. The received pulse shape $I_R(x)$ is used as a probability function for distributing the n photoelectrons determined in step 5. The pulse shape is integrated and divided by the total energy to give the normalized energy E as a function of x. Each element of energy has an equal probability of generating a photoelectron. A random number generator giving random numbers uniformly distributed on the interval 0 to 1 is used to pick n points along the energy axis. By inverting the function $E(x)$ to give $x(E)$ one obtains n values of x giving the positions of the photoelectrons.

7. The output pulse $f(x)$ of the photomultiplier is constructed as the sum of Gaussian pulses resulting from each photoelectron.

$$f(x) = \sum_{i=1}^{n} A e^{-\frac{x^2}{2\sigma_p^2}}$$

where A = amplitude of the single photoelectron signal
    σ_p = sigma of the single photoelectron signal
        = $\tau_{pm}/(2 \times 1.28)$
    τ_{pm} = photomultiplier rise time

8. The centroid of the pulse is computed as

$$\text{Centroid} = \frac{\int_{-\infty}^{\infty} x f(x) dx}{\int_{-\infty}^{\infty} f(x) dx}$$

The half area point is the point x for which

$$\int_{-\infty}^{x} f(x) dx = \frac{1}{2} \int_{-\infty}^{\infty} f(x) dx$$

9. The pulse height analyzer is simulated by integrating the pulse over .8 nanosecond intervals and assigning the value F of each interval to the midpoint of the interval x. The analyzer centroid of the pulse is then

$$\text{Analyzer} = \frac{\sum_{i=1}^{20} F_i x_i}{\sum_{i=1}^{20} F_i}$$

The width of the integration interval (.8 ns above) and the spacing of the points x_i are controlled by input parameters as well as the number of channels which is usually 20 or 40. The first channel is to the right ($+x$ direction) and the last is to the left ($-x$ direction). The positioning of the first channel is determined by requiring that the start of the 7th (or other channel specified on input) be at the half-max point on the pulse.

The half maximum detection system is simulated by starting from the $+x$ end of the pulse and finding the first point where $f(x)$ is half of the maximum value of $f(x)$. Fixed thresholds are done similarly for various constant values of the threshold.